An Experimental Study of Molten Microdroplet Surface Deposition and Solidification: Transient Behavior and Wetting Angle Dynamics

D. Attinger

Z. Zhao

D. Poulikakos

Laboratory of Thermodynamics
in Emerging Technologies,
Institute of Energy Technology,
Swiss Federal Institute of
Technology (ETH),
8092 Zurich, Switzerland

The basic problem of the impact and solidification of molten droplets on a substrate is of central importance to a host of processes. An important and novel such process in the area of micromanufacturing is solder jetting where microscopic solder droplets are dispensed for the attachment of microelectronic components. Despite the recent appearance of a few numerical studies focusing on the complex transient aspects of this process, no analogous experimental results have been reported to date to the best of our knowledge. Such a study is reported in this paper. Eutectic solder (63Sn37Pb) was melted to a preset superheat and used in a specially designed droplet generator to produce droplets with diameters in the range 50–100 μm. In a first series of experiments, the size, temperature, and impacting speed of the molten droplets were maintained constant. The primary variable was the temperature of the substrate that was controlled in the range from 48°C to 135°C. The dynamics of molten solder microdroplet impact and solidification on the substrate was investigated using a flash microscopy technique. The time for the completion of solidification from the moment of a solder droplet impact on the substrate varies between 150 μs and 350 μs. The dynamic interaction between the oscillation in the liquid region and the rapid advance of the solidification front was visualized, quantified, and presented in this paper. In a second series of experiments, the evolution of the wetting angle between the spreading drop and the substrate was recorded and analyzed. No quantitative agreement with Hoffman's correlation for wetting was found. It was established that the wetting angle dynamics is strongly coupled with the evolution of the droplet free surface. Two successive regimes were distinguished during the spreading. The influence of the initial impact velocity and substrate temperature on the dynamics of the measured wetting angle was described in both regimes. To the best of our knowledge, this study presents the first published experimental results on the transient fluid dynamics and solidification of molten microdroplets impacting on a substrate at the above-mentioned time and length scales that are directly relevant to the novel solder jetting technology. [S0022-1481(00)01403-1]

Keywords: Droplet, Heat Transfer, Manufacturing, Microscale, Visualization

1 Introduction

Scientific research interest on droplet-surface interactions has recently increased, driven by a need for an in-depth understanding of new aspects of droplet impact phenomena that are important to emerging technologies such as spray deposition ([1,2]) and picoliter size solder droplet dispensing. Picoliter size droplet dispensing (the application to which the present work is directly relevant) is used for advanced surface mount technologies (SMT) in the packaging of electronic microchips. In this technology, monodispersed arrays of molten metal microdroplets (25–100 μm in diameter) are printed on a substrate, each microdroplet (or bump) forming an electrical connection. Important advantages of picoliter size droplet dispensing over other bumping technologies are the flexibility and low cost, because neither masks nor screens are required ([3,4]).

Many physical phenomena related to the prediction of bump shape and metallic properties are not well understood. There is still a lack of basic understanding and modeling capabilities for phenomena, such as the dynamic behavior of the wetting angle between the substrate and the droplet ([5]), the thermal contact resistance between splat and substrate as well as the rapid solidification phenomenon ([6]), including heterogeneous nucleation and recalescence, as well as the possible remelting of the substrate ([7]). These are typical mesoscopic phenomena, whose physics is often related to microscopic phenomena and cannot be understood using the classical continuum approach. A common way to handle these mesoscopic phenomena is to match experiments with numerical or analytical models in order to estimate the needed model parameters. Using this approach, several temperature measurements under relatively large (mm size) solidifying droplets have been performed and matched with numerical simulations in order to estimate the values of the thermal contact resistance between the splat and the substrate ([8–10]) or to estimate the nucleation temperature ([8]).

The evolution of the wetting angle during droplet spreading also contains largely unresolved physics. The wetting angle behavior at the molecular level is governed by intermolecular forces ([11]). The relation, if any, between the molecular angle and the macroscopic angle (visible with a low-power microscope, and measured in the present study) is also not well established ([12]).

Contributed by the Heat Transfer Division for publication in the JOURNAL OF HEAT TRANSFER. Manuscript received by the Heat Transfer Division, Oct. 25, 1999; revision received, Apr. 11, 2000. Associate Technical Editor: T. Avedisian.

 Copyright © 2000 by ASME

Empirical correlations, such as Hoffman's law ([13]), express the dynamic evolution of the macroscopic wetting angle α as a function of the capillary number Ca and of the equilibrium wetting angle α_{eq}, for steady flows under conditions of negligible Weber number ([12]). In the impact of a droplet on a flat surface, the fluid dynamics is unsteady and the Weber number based on the contact line velocity is not negligible. Therefore, the motion of the droplet free surface near the contact line and the dynamics of the bulk fluid may influence the value of the wetting angle. Furthermore, in a molten droplet impact, there is the additional contribution of heat transfer, which can drastically change flow properties by glassification, or can even arrest the motion of the contact line by solidification. Fukai et al. [14] and Pasandideh-Fard et al. [9] used experimentally measured advancing and receding wetting angles in their numerical models to study the effects of surface wetting on the spreading and recoiling motion of a droplet after impingement on a dry surface. However, since these angles and substrate temperatures have been measured for rather larger systems, with respect to both time and space scales, the question arises if the conclusions can be applied to smaller scales of the kind found in picoliter size solder droplet dispensing and spray casting.

A promising approach to obtain direct insight in the thermophysics of picoliter-size molten droplet impact is the high-speed visualization of such a process. If it were possible to observe, with enough time and space resolution, the spreading and solidification dynamics of picoliter solder droplet impact, in addition to the direct information that the experiments would provide, a comparison with numerical studies of the same problem, such as those by Waldvogel and Poulikakos [15] and by Xiong et al. [16], would be feasible. Such experiments are reported in the present paper. A key finding of the above two papers is that a strong coupling occurs between heat transfer, fluid dynamics, and phase change, leading to a wavy surface of the solder bumps. Although this wavy surface appears in both numerical and experimental studies (the latter yielding only the shape of the completely solidified microbump), there is still a significant discrepancy between numerical results and final shape micrographs ([16]). A visualization of the microdroplet in motion accompanied by relevant quantitative measurements contributes significantly to the understanding of this phenomenon.

A variety of visualization techniques have been applied in the experimental investigations of droplet impact dynamics, including high-speed camera techniques ([17–21]), flash photography ([22–24]), and flash videography ([25–26]). There is one basic distinction between high-speed camera and flash techniques: the former records the highest number of frames from a single event, while the latter reconstructs the event by patching together several frames taken at different instants from several reproducible events. In our case, the expected short duration of the phenomenon (of the order of 100 microseconds) prevented the use of most high-speed cameras. For example, even a very fast CCD camera such as the Kodak EKTAPRO (40, 500 partial frames per second and available in our laboratory) could only give a rough qualitative recording of the phenomenon. Intensified CCD cameras have a time delay between two frames smaller than 50 ns and could have solved the time resolution problem. However, this expensive technology only allows recording a limited number of frames (8 to 30) of a single event ([27]) so that the reconstruction problematic of one event from several reproducible events would have arisen in this case as well. The high-speed 16-mm camera technique has not been considered because of its complex machinery, high costs, and difficulty of implementation ([28]).

In contrast with the methods discussed above, the flash photography and flash videography techniques are stroboscopic methods whereby a variable number of short-pulse illuminations (1 to 10 pulses) are produced at specific instants during each event and recorded by a 35-mm camera or a CCD camera, respectively. By generating a sequence of identical drops and practically identical impact events per drop, one can capture different stages of the process in each event and piece together from images of droplets taken at progressive stages the entire impact, spreading, and solidification process. Key parameters describing the droplet spreading process, i.e., splat/substrate contact area, splat diameter, and thickness as well as the wetting angle ([9]), can be subsequently measured from the recorded pictures of spreading droplets. The flash techniques rely therefore on the generation of droplets in a highly repeatable manner ([22,25,24,26]) since the impact process is reconstructed from images of several impact events.

Good quality images of a droplet spreading process have been reported in the literature using short-duration flash photography ([22,9]) for millimeter-size droplets, and flash videography ([26]) for droplet diameters of the order of 60 μm to about 1 mm. To exemplify, the study of Pasandideh-Fard et al. [9] reports a visualization of impact and solidification of relatively large (approx. 2 mm) liquid metal tin drops on a cold substrate. Hence, the resulting Weber number value of We=71 does not correspond to the relatively low Weber domain ($4<\mathrm{We}<10$) encountered in picoliter size solder droplet dispensing that is the focus of the present research. In the present study a flash videography technique, coupled with a digital grabbing of the images for the ease of postprocessing, is developed and implemented.

2 Experimental Setup

2.1 Molten Solder Microdroplet Deposition System. To investigate the dynamic process of impact and solidification of picoliter size molten metal droplet on the surface of a semiconductor device, a molten solder microdroplet jetting device was set up at ETH Zurich with technical assistance from MicroFab Technologies Inc. (Dallas, TX). The method used for the generation of monodispersed picoliter-size droplets of solder at demand with the potential of use in the manufacturing of electronic components was described in ([3]) and ([29]), and is summarized as follows.

By applying an electric pulse to a piezoelectric material not in direct contact with the fluid, picoliter volumes of molten metal are ejected from an orifice at demand in accordance with the electric pulse frequency. After oscillating, the ejected tiny amount of metal assumes a spherical shape due to minimization of surface tension energy. The process is termed solder jetting at demand. The jetting apparatus used in the present study is shown schematically in Fig. 1.

Solder is melted in an enclosed reservoir by resistance heating. The molten solder reservoir is pressurized with nitrogen to insulate the melt with a chemically inert environment and provide back pressure for jetting. A nitrogen flowing as a curtain around the path of the droplet toward the substrate limits the interaction with the surrounding air and prevents, at least to a good extent,

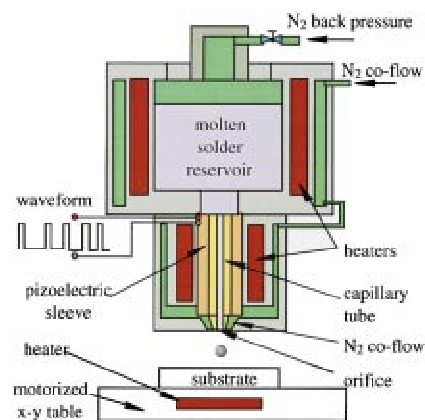

Fig. 1 Schematic of the picoliter size solder droplet deposition apparatus

droplet oxidation. Molten solder temperatures in the reservoir and the capillary tube are both monitored by thermocouples and controlled through the heaters. The waveform of the drive pulse for solder jetting is electronically generated and digitally controlled. By varying the waveform, the diameter and the velocity of ejected solder droplets can be altered in the ranges of 50–100 μm and 1–2.5 m/s, respectively. The alloy used in this study is a eutectic tin lead solder (63 percent Sn-37 percent Pb) with 99.99 percent purity, specially developed for solder jetting by Witmetaal B. V., Holland. Delay time between droplet ejection can be changed by varying the waveform driver frequency for droplet generation. However, the repeatability of droplet diameter and ejection velocity is greatly improved when the frequency of droplet ejection is maintained constant during the experiment. In the present study, a droplet generation frequency of 12 Hz was used.

After ejection from the orifice, a solder droplet travels approximately 1 mm and impacts the substrate mounted horizontally on a motorized *x-y* precision stage (Photon Control PTS 1000, England). The substrate in the present study is a semiconductor wafer (EM Marin, Switzerland) cut to a die size of approximately 10×50 mm. The wafer consists of the following layers from top to bottom: 0.1-μm-thick Au, 0.3-μm Ti90W alloy, 1-μm silicon nitride (conductivity $\lambda = 2.33(+-0.11)\ \mathrm{Wm^{-1}K^{-1}}$, heat capacity $\rho c_p = 2.62(+-0.22)*10^{-6}\ \mathrm{Jm^{-3}\,K^{-1}}$) ([30]) and 675-$\mu$m P-silicon. The substrate wafer slide is mounted on a heated copper plate with a thin layer of thermal interface paste (HTC Electrolube, England) between the wafer and the copper plate, with $\lambda = 0.84\ \mathrm{Wm^{-1}\,K^{-1}}$. The wafer top ($T_{2,0}$) and bottom ($T_{3,0}$) surface initial temperatures are measured with two K-type thermocouples (Omega 304 SS9), the former being epoxied on the wafer with a 1-mm-size island of conductive epoxy (AV138M/HV998 Novartis, Switzerland) with $\lambda = 0.6\ \mathrm{Wm^{-1}\,K^{-1}}$. The bead diameter of the thermocouples is 250 μm. The copper plate temperature was PID-controlled to vary $T_{2,0}$ between 48°C and 135°C. Since the wafer slides used in printing have to be frequently replaced, the temperature measurements are carried out on another wafer slide, permanently deposited on the copper plate, and moved under the printhead at the same conditions as the wafer slide where droplets impact. Both radiation from the metallic parts of the printing device and convection from the co-flow increased significantly the wafer temperatures. The *x-y* stage motion (2 mm/s) is so slow that the thermocouples reach a steady-state value before passing under the jet orifice and maintain it after passing by the jet orifice. Therefore the transient temperature effect is considered to be negligible.

2.2 Visualization of Solder Droplet Deposition Using Flash Videography. As described in the Introduction, the technique used for the visualization of droplet impact and solidification is a flash videography technique ([26]) where only one image is taken at one instant during the impact and solidification process for each drop studied. The imaging system used to record the droplet deposition process is shown schematically in Fig. 2.

Backlighting for the first series of experiments is provided by a Xenon flash light unit (Hamamatsu L4634). The flash energy is 0.15 J/flash and the duration of each burst of flash is 1 μs with less than 200 ns jittering. The time resolution of the sequence recording is set to 5 μs. A Fresnel lens is used to provide uniform and intensified (focused) backlighting field for the microscope. The droplet images are magnified using a microscope objective (Microtech Zoom 70, USA) with $29\times$ optical magnification on the CCD matrix plane, which provides a space resolution of 1.2 μm in the object plane. The conditions for the wetting angle measurement are slightly different from the first experiments in this paper. The optical magnification is increased up to 36 times. In order to capture the fast kinematics during the beginning of the spreading (with contact line velocities of the order of 2 to 4 m/s), a faster Xenon flash light unit (FX-HSPS, Wedel, Germany) is employed. It provides a shorter flash duration of 150 ns with less than 60 ns

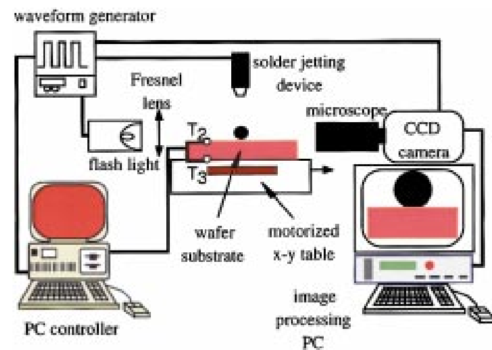

Fig. 2 Flash videography technique used for recording the solder droplet deposition process

jittering, with a flash energy of 0.1 J/burst. The time resolution of the sequence recording is also increased up to 300 nanoseconds during the first stage of the spreading.

Images of the droplets are acquired with a Jai M10 progressive scan CCD camera (Denmark) in triggered mode and are digitized and stored in the image processing PC. An example of the picture quality of a droplet in motion is given in Fig. 3(*b*). As a result of high power optical magnification, the ambient light introduces little optical noise on droplet images, and the flash light acts therefore as a shutter. The waveform generator that activates the solder

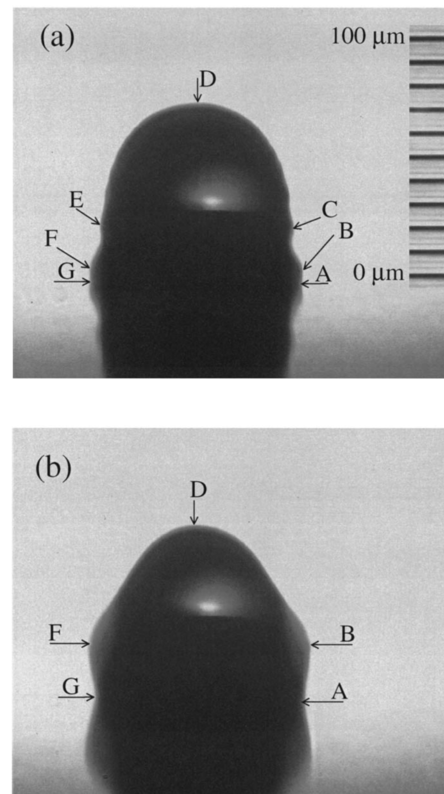

Fig. 3 Measured points on the droplet surface. Points A and G determine the droplet wetting area diameter. D is the highest visible point of the surface, when viewing from the side, not always at the axis of symmetry. The distance from D to segment AG determines the visible droplet height H above the surface (identified by the segment AG). The shadow below the surface and the light spot inside the droplet are optical effects. The accuracy in determining the vertical and horizontal position of A and G decreases for wetting angle values near 90 deg, and larger than 110 deg, respectively.

jetting device sends a signal with a preset delay to trigger the flash light when a solder droplet hits the substrate. To record the progressive stages of solder droplet spreading and solidification, the delay time between droplet ejection and a burst of back lighting is increased between successive images.

In order to provide a free impact surface for each impinging droplet, the motorized *x-y* stage is maintained at a constant linear speed of 2 mm/s in the focal plane of the microscope during experimental runs. This translation velocity of 2 mm/s is about three orders of magnitude smaller than the impact velocity of 1.5 m/s. In a reference frame attached to the translation stage, this motion corresponds to a deviation from the vertical direction of the impact smaller than 0.1 degrees, thus negligible.

2.3 Image Analysis and Discussion of the Experimental Uncertainties. Image analysis is carried out using an image processing software (Optimas 6.2, Media Cybernetics, USA) that allows the measurement of droplet area and the motion analysis of selected points for a sequence of images. Figure 3 shows a measurement example of droplet wetting area diameter (distance between A and G) and droplet height (distance from point D to segment AG). It should be emphasized that such measurements involve uncertainties, due to the human identification of the measured points. In the case of clearly defined points such as in Fig. 3(*b*), 20 measurements of the points on the same image yield a standard deviation (in percentage of the initial droplet diameter) of 0.06, 0.54, 0.91, 0.44 and 0.16 percent for the vertical position of D, the distance between D and segment AG, and the position of the single points A and G, as well as the wetting area diameter, respectively. It is worth noting that a wetting angle α larger than 110 deg can cause significant optical blurring (as in Fig. 4, 30 μs), and therefore increase the error for the wetting area diameter.

The choice of a flash videography technique that consists of building an impact sequence from a series of single pictures, each of them taken from a different droplet requires a highly reproducible process. There are several factors that can influence the reproducibility of droplet release and solidification. We examined, with the setup used for the first series of experiments, two possible perturbation sources, i.e., the stability in the drop position and velocity as well as the importance of the wafer heating due to the heat released by solidification of the previous drop.

The positions of the top, bottom, left, and right extreme points of 99 solder droplets in the same conditions as in the experiment have been measured with a constant delay between ejection and flash. The standard deviation in the horizontal position of the extreme right and left position is, respectively, 1.32 percent and 1.46 percent of the diameter (80 μm), and the standard deviation in the vertical position for the top and bottom points is 2.2 percent (± 1.76 μm) and 1.72 percent, respectively. The maximum standard deviation in the vertical position corresponds to a jitter in the droplet ejection of ± 1.17 μs. Since this error is markedly larger than the error due to the human identification of the measured points, the major cause of uncertainties in the measurements is due to the needed repeatability of the visualization technique.

The magnitude of wafer slide heating due to the heat released by solidification of the previous drop has been evaluated in two ways. First, we estimated the final increase in the wafer temperature after the impact of a series of droplets that corresponds to our experimental conditions. Then, we estimated if the transient local heat release of a previous drop would affect the initial conditions for the actual drop. The final temperature increase was estimated as follows. Assuming that the heat released by the drops increases the wafer temperature uniformly, we express the temperature increase ΔT of a typical wafer slide (10 mm by 50 mm surface):

$$\Delta T = \frac{nE_Q}{\sum_i \rho_i V_i c_{pi}} \tag{1}$$

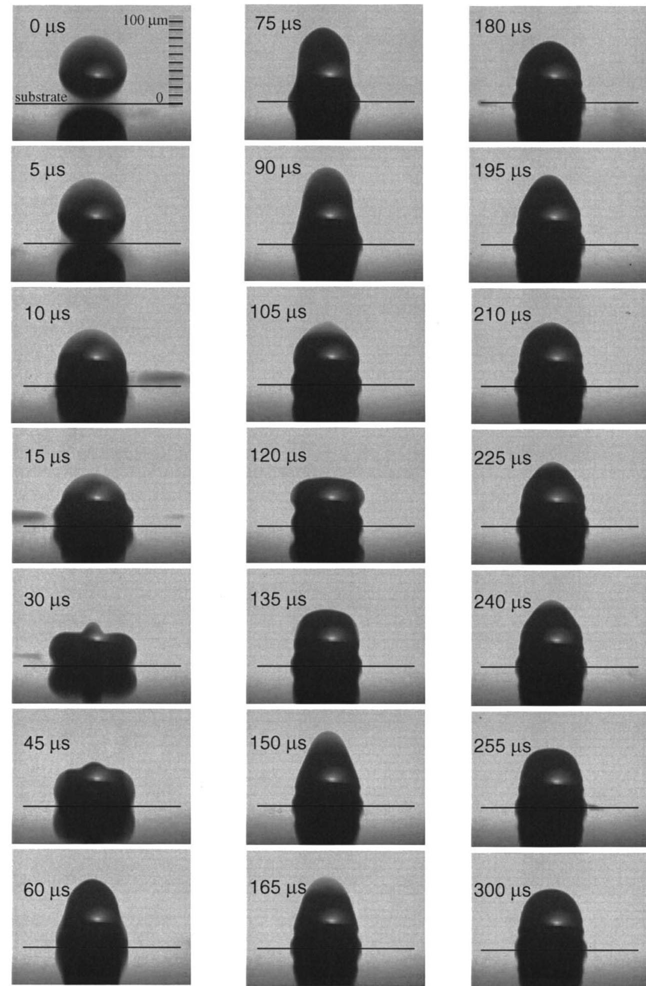

Fig. 4 Spreading, oscillations, and freezing of a solder droplet on a flat substrate. Initial conditions: $v_0 = 1.54$ m/s, $d_0 = 80$ μm, $T_{1,0} = 210°$C, $T_{2,0} = 48°$C.

where n, E_Q, ρ, V, and c_p are the number of droplets, the heat released by droplet solidification and subcooling, the density, volume, and heat capacity of each layer i of the wafer. In the case where 300 droplets (i.e., 3 sequences of 100 drops) at 210°C impact a wafer slide of the same composition as the one used in the experiments, we maintain that the wafer temperature increase ΔT is less than 0.1K, and is thus negligible. The transient effect of the previous droplet impact on the actual drop can be calculated accurately numerically, but we obtained an acceptable estimate by assuming that the entire E_Q is released at time $t=0$ in a half-sphere of an infinite radius. In other words, we consider that each droplet acts as an instantaneous heat source on the surface. In this case, an analytical relation exists for the temporal and local evolution of the temperature ([31]). Considering a pitch distance between droplets of 166 micrometers (corresponding to a printing frequency of 12 Hz), the maximum transient temperature variation due to heat released by the previously impacting droplet for a distance of 166 micrometers from the heating source, was found to be 0.03 K in a gold hemisphere and 0.13 K in a silicon hemisphere, and is thus negligible.

A further difference between the experiments and the ideal case of a spherical droplet impinging on a substrate is that there are still small residual shape oscillations from the ejection process at the instant of impact. Hence, the droplet shape at the time of impact is not absolutely spherical. This error can be estimated by observing the maximum error in nonsphericity on the pictures

right before impact: At the distance used for printing, the diameter oscillation amplitude was ±5 percent of the droplet diameter. A series of measurements showed that the phase lag between the oscillations of the horizontal diameter and the vertical diameter equals π, thus this oscillation should not influence the measurement of droplet size, based on the visible area. Accordingly, the measurement of droplet velocity before impact was based on the motion of the two points at the extreme left and right of the droplet. Their height is a bit more difficult to determine than, for example, the height of the bottom point of the droplet, but it does not oscillate in the vertical direction.

Table 1 Initial conditions for the first series of experiments pertaining to the overview of the spreading and solidification process

v_0(m/s)	1.52 ± 0.06					
$T_{2,0}$(°C)	48	62	81	98	118	135
Re	381					
We	4.4					
Ste	0.77	0.69	0.58	0.48	0.37	0.27
Oh	0.0055					
Pt	0.025					

3 Results

3.1 Experimental Conditions. Two series of experiments were performed. The first series was focused on the transient behavior of the spreading and solidification process. The second series was focused on the wetting angle dynamics. In the first series, sequences of molten solder microdroplet impingement on a colder wafer, such as those shown in Figs. 4 and 5, have been recorded for different initial temperatures of the top surface of the wafer ($T_{2,0}$=48, 62, 81, 98, 118, and 135°C). The temperature $T_{3,0}$ of the bottom surface of the wafer was measured to be in each case 5 to 6 K lower than $T_{2,0}$. Each sequence was reconstructed from about 100 frames, the delay between drop release and flash being increased in steps of 5 μs between each frame. In each sequence, the time $t=0$ corresponds to the last picture before impact. The maximum corresponding error in determining the time $t=0$ when the droplet contacts the substrate is therefore 5 μs. The produced drops had a mean diameter d_0 in the range of 79.7 to 83.9 μm and a velocity v_0 in the range of 1.49 to 1.58 m/s, with average values of 81.4 μm and 1.52 m/s, respectively. The characteristic numbers, defined in the Nomenclature, are shown in Table 1. They are based on the following values for the thermophysical properties: $\sigma=0.345\,\mathrm{Jm}^{-2}$, $\mu=0.00262\,\mathrm{Pa\,s}$, $L=42{,}000\,\mathrm{J/kg}$, $c_{pl}=238\,\mathrm{J\,kg}^{-1}\,\mathrm{K}^{-1}$, $\lambda_1=25\,\mathrm{Wm}^{-1}\,\mathrm{K}^{-1}$, and $T_m=183°\mathrm{C}$, and on the average measured values of velocities and diameter.

The second series of experiments, focusing on the evolution of the wetting angle, was performed with a more precise lighting, an increased optical magnification, and time resolution, as described above. Four sequences of data were collected, where the surface temperatures and the initial impact velocities were varied as shown in Table 2. The mean value of the initial diameter d_0 was slightly smaller than in the first series of experiments ($74.1\pm2\,\mu$m), and has been used for the calculation of the Reynolds and Weber numbers. The remaining experimental conditions were the same as in the first series of experiments.

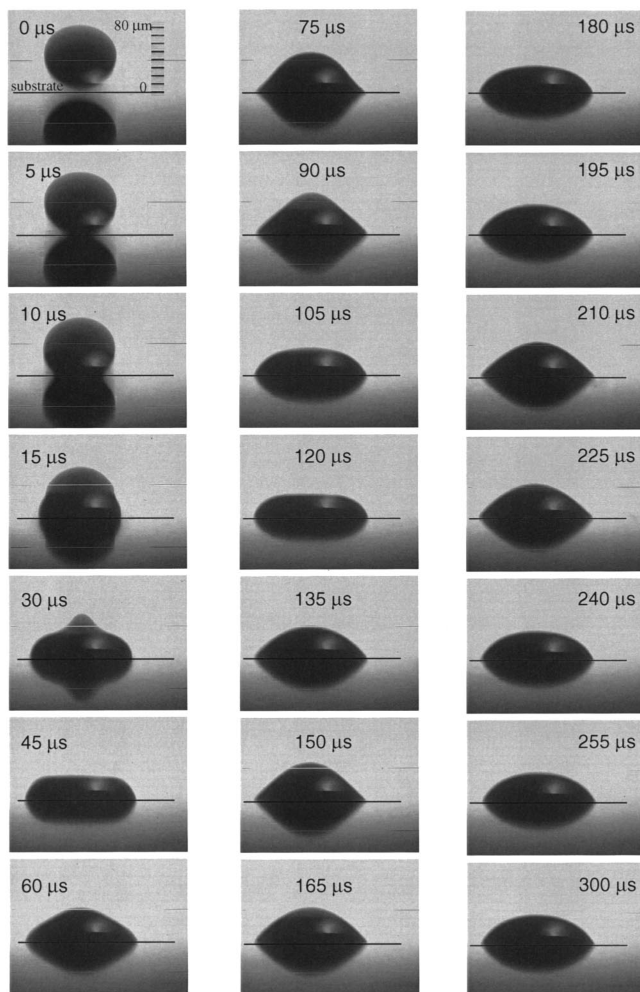

Fig. 5 Spreading, oscillations, and freezing of a solder droplet on a flat substrate. Initial conditions: $v_0=1.49$ m/s, $d_0=84\,\mu$m, $T_{1,0}=210°$C, $T_{2,0}=135°$C.

3.2 Qualitative Investigation of the Spreading and Solidification Process. Figure 4 shows a reconstructed sequence corresponding to an initial wafer temperature $T_{2,0}$ of 48°C. A qualitative inspection of Fig. 4 reveals that the spreading time (defined as the time taken by the droplet to spread to its maximum contact area) is approximately 30 μs.

The subsequent contour shapes caused by the upward motion of the droplet fluid indicate that the fraction of solidified mass is small within the first cycle of the droplet oscillation. The large variation of droplet height during the subsequent oscillation also suggests that the damping effect of viscous force is less important than the effect of surface tension force.

In the case of impact on a substrate with We>1, the radial pressure gradient induced by the impact drives the process of droplet spreading ([6,32,5,33]). Surface tension forces, liquid viscous forces, and solidification work together to arrest the droplet spreading. According to Bennett and Poulikakos [32], surface tension effects dominate the termination of droplet spreading over viscous effect when

$$\mathrm{We}\ll 2.8\,\mathrm{Re}^{0.457}. \tag{2}$$

For the droplet impingement conditions in Fig. 4, the right-hand side of the above equation has a value of 42.3. Comparison with

Table 2 Initial conditions for the second series of experiments focusing on the evolution of the wetting angle

v_0 (m/s)	2.35	2.31	1.49	1.51
$T_{2,0}$(°C)	145	59	65	119
Re	546	537	348	350
We	9.7	9.4	3.9	4.0
Ste	0.22	0.70	0.67	0.36
Oh	0.0057	0.0057	0.0057	0.0057
Pr	0.025	0.025	0.025	0.025

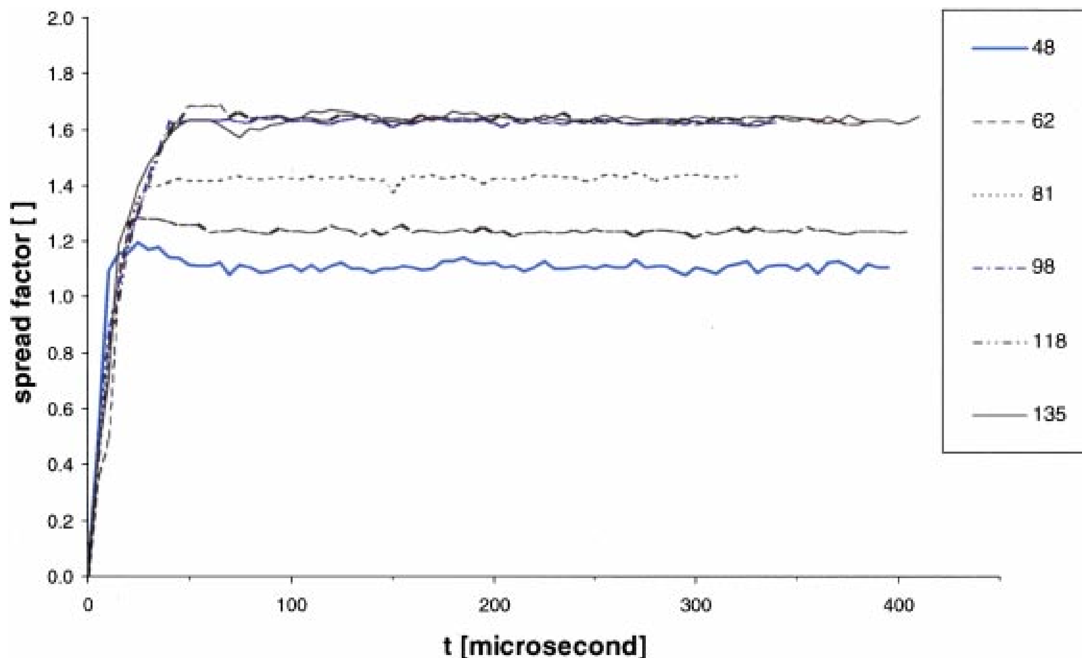

Fig. 6 Time evolution of the spread factor β, with the substrate temperature $T_{2,0}$ as a parameter. The error is estimated in Section 2.3.

the Weber number, about ten times smaller, indicates that the condition for the droplet deposition shown in Fig. 4 is well into the surface tension domain concerning the relative influence of viscous dissipation and surface tension.

Solidification effects can influence droplet motion ([33]). Neglecting the presence of contact thermal resistance between the substrate and the droplet bottom, the ratio of spreading time, t_{spr}, to the solidification time, t_s, can be estimated from ([33])

$$t_{spr}/t_s = \text{OhSte/Pr}. \tag{3}$$

The ratio calculated from the above equation is 0.17, indicating that the droplet spreading time is smaller than the solidification time. It is expected that the above ratio will be further reduced in the presence of interface thermal contact resistance. According to Fig. 4, the spreading time is approximately 30 μs before the recoiling motion in the liquid region. No changes of the droplet shape are visible for the points located at the top of the droplet contour after 255 μs. Assuming that the arrest of droplet oscillatory motion is caused by solidification and not by viscous damping (which is reasonable since four visible ripples on the drop surface indicate that solidification arrested most of the drop motion), the ratio of the measured droplet spreading time to solidification time is 0.12. This agrees relatively well with the prediction of Eq. (3).

While droplet solidification is significantly slower than droplet spreading as shown above, it is also obvious that the subsequent oscillatory motion of the droplet is strongly affected by solidification. First, it can be shown by counting the number of frames for each oscillatory cycle that the oscillation frequency is increased with the upward propagation of the droplet solidification front, which reduces the total liquid mass of the droplet. Numerical simulations suggested that the oscillation frequency of an impacting droplet is closely related to the droplet natural frequency ([34])

$$f \propto (\sigma/\rho_l V_l)^{1/2} \tag{4}$$

where V_l is the liquid volume. As the solidification front propagates into the molten region, the remaining liquid mass of the droplet decreases, which results in an increase of the oscillation frequency. Second, Fig. 4 confirms that the ripples visible on the drop surface are due to a strong coupling between solidification and oscillations, which was suggested by numerical results pertaining to a comparable parameter range ([15,16]).

Solidification can influence the spreading. This occurs by freezing at the wetting line ([35]), or by destruction of kinetic energy by solidification ([9]). The parameter measuring the spreading is the spread factor, β, defined as the ratio of the diameter d of the wetted substrate area over the initial droplet diameter d_0. A comparison between Figs. 4 and 5 shows a significant increase of the maximum spread factor β_{max} when the substrate temperature is increased to 135°C. Assuming heat transfer between the substrate and the droplet only affects the spreading by delaying the solidification start ([6,33]), the increase of β_{max} with increasing substrate temperature shows that solidification influences the spreading.

Other effects caused by an increase in the substrate temperature are visible in comparing Figs. 4 and 5. The final height decreases and ripples are no longer visible: the droplet assumes a lens shape. These and other phenomena are discussed in the next section, which considers measurements from pictures of droplet spreading for increasing initial substrate temperatures.

3.3 Quantitative Investigation of the Spreading and Solidification Process. The time evolution of the spread factor β, measured as in Fig. 3, is shown in Fig. 6 with the substrate initial temperature $T_{2,0}$ as a parameter. The time resolution is 5 μs. In the first 15 μs after impact, β increases from 0 to about 1 in a similar way for all values of $T_{2,0}$ examined. However, the attained final values β_∞ depend markedly on $T_{2,0}$. These final values increase with substrate temperature for $T_{2,0}$ between 48 and 98°C, and are almost constant for higher temperatures. The dynamic nondimensional parameters of impact, including We, Re, and Oh numbers, are approximately the same in every case. The difference is the thermodynamic parameter for phase change, the Stefan number, calculated in Table 1. The similar behavior of $\beta(t)$ for $T_{2,0}$ in the range 98 to 135°C indicates that above 98°C (i.e., below Ste $=0.48$), there is no dependency of β on the Stefan number. This implies that solidification does not influence the spreading for $T_{2,0}$ over 98°C. Therefore, the assumption that the droplet spreads first and solidifies subsequently appears to be valid in this range of

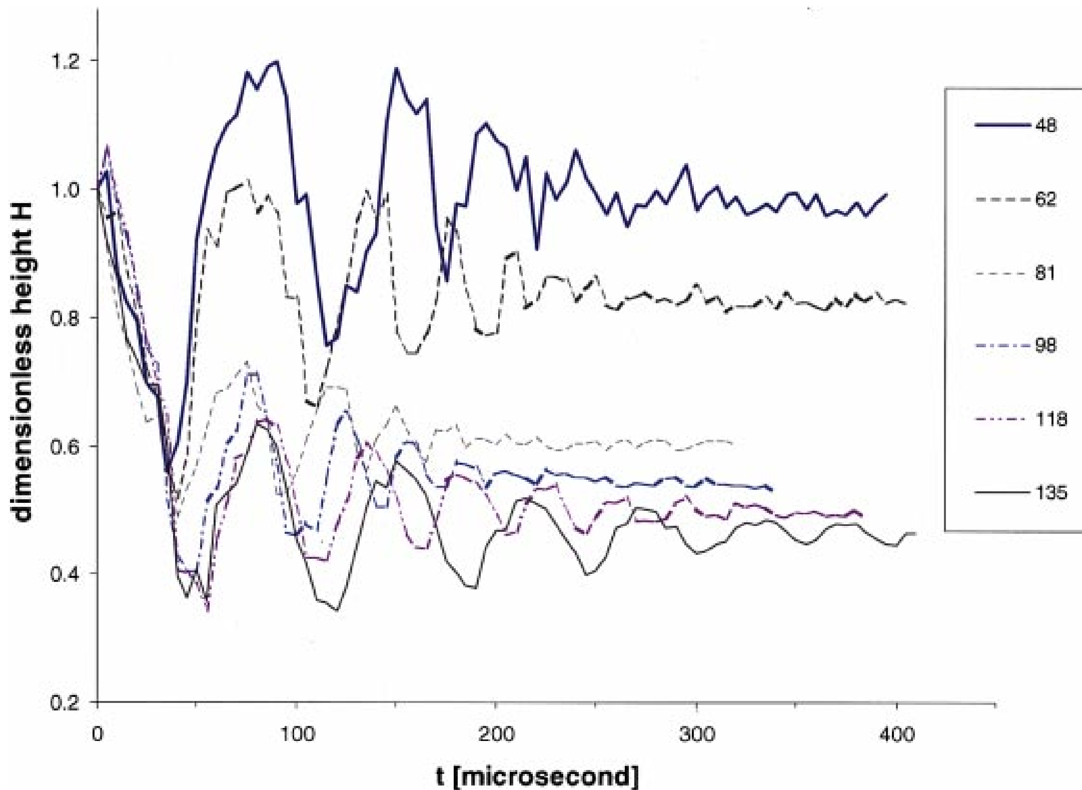

Fig. 7 Time evolution of the dimensionless visible droplet height over the substrate *H*, with the substrate temperature $T_{2,0}$ as a parameter. The error is estimated in Section 2.3.

$T_{2,0}$. This is indicated by the good agreement between the final spread factor we measured for $T_{2,0}$ above 98°C ($\beta \approx 1.6$) and results from an analytical relation of Pasandideh-Fard et al. [36]. This relation estimates the maximum spread factor in the absence of solidification to be 1.65 with our mean values of Re, We, and with an advancing wetting angle value of 135 deg in the early stages of spreading. It is worth noting that the above analytical relation is based on the assumption of a reasonably high Reynolds number, so as to produce a thin boundary layer in the liquid as it spreads, which is only partially valid in our case (Re=381). We found it interesting that this relation predicts within five percent the spreading ratio of our measurements in the absence of solidification (i.e., when the substrate initial temperature is high). This is why we have tested the extension of this relation ([9]) that considers solidification effects by assuming that the influence of solidification is manifested by kinetic energy destruction. In this case, the model results do not agree well with our experimental results. The calculated maximum spread factors lie between 1.52 and 1.57, and our experimental values are between 1.20 and 1.69. One possible reason for this discrepancy could be that solidification influences the spreading by arresting the wetting line via freezing rather than by destroying kinetic energy. In a published numerical study pertaining to the same parameter range as this experimental study, Waldvogel and Poulikakos [15] have shown that freezing at the wetting line controls wetting line arrest. This has also been observed experimentally by Schiaffino and Sonin [35] for low Weber numbers. However, the history of the spread factor β for the lowest substrate temperature $T_{2,0}=48$°C (Fig. 6) shows a maximum value of β significantly bigger (eight percent) than the final value of β. This measurement, concerning the highest Stefan number (0.77) of our measurement range, would contradict the hypothesis that freezing at the wetting line controls the maximum spreading. This apparent contradiction is probably a consequence of the significant blurring at the contact between splat and substrate in Fig. 4 (30 μs), which makes the accurate measurement of the maximum spread factor difficult.

Figure 7 shows the time evolution of the dimensionless visible droplet height *H* over the substrate (defined in Fig. 3 as the maximum height when viewing from the side at any time instance), with $T_{2,0}$ as a parameter. It should be emphasized that the visible droplet height does not always correspond to the height of the intersection of the axis of symmetry with the free surface. For example, simulations by Waldvogel and Poulikakos [15] have shown that, in the early stages of the spreading, the height of the intersection of the axis of symmetry with the free surface is smaller than the droplet height visible from the side. The motion of the droplet height shown in Fig. 7 can be termed as a damped oscillation. Figure 8 shows the final, maximum and minimum values of the visible droplet height, each corresponding to a fixed

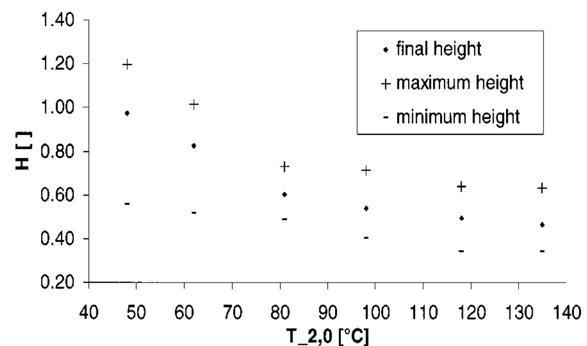

Fig. 8 Final, maximum and minimum droplet nondimensional visible height *H* as a function of $T_{2,0}$. The error is estimated in Section 2.3.

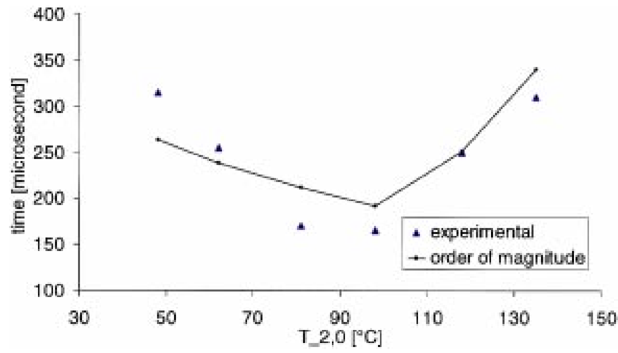

Fig. 9 Solidification time t_s as a function of $T_{2,0}$. The experimental values refer to the apparent solidification time, and the order of magnitude values refer to Eqs. (5) to (8).

substrate temperature. The maximum visible height is measured from the beginning of first recoiling, and the final visible height is measured by averaging the height of the ten last frames of each visualization series. The final maximum and minimum values of the visible droplet height decrease monotonically with $T_{2,0}$. At temperatures below 98°C, the monotonical decrease of final height with substrate temperature can be correlated with the increase of $\beta_{\max}$ with substrate temperature (Fig. 6).

Quantitative information about the solidification time has been extracted from Fig. 7 as follows. We assume that the droplet is frozen when the droplet height remains constant (within ± 2 percent of the initial diameter) for a time length more than half a period of its oscillations (corresponding to a series of ten successive frames). The apparent solidification time is then defined arbitrarily as the time of the first frame of the above mentioned series. The apparent solidification time is represented in Fig. 9. It depends nonmonotonically on $T_{2,0}$, with a minimum of about 165 μs at $T_{2,0} = 98$°C. This nonmonotonic dependence of the apparent solidification time on $T_{2,0}$ indicates a nonmonotonic dependence of the effective solidification time on $T_{2,0}$, as calculated in previous numerical simulations ([15,16]). An order of magnitude explanation of this nonmonotonic dependence of the solidification time on $T_{2,0}$ is presented hereafter. If we neglect the effect of superheat and subcooling, we can consider that the energy E_s released by the solidification of the droplet is constant with respect to $T_{2,0}$:

$$E_s = \rho V L. \tag{5}$$

The solidificaiton time t_s is expressed as follows:

$$t_s = \frac{E_s}{\dot{q}}. \tag{6}$$

We also assume that the heat flux $\dot{q}$ can be expressed by

$$\dot{q} = h_e S (T_m - T_{2,0}) \tag{7}$$

where h_e is an effective heat transfer coefficient and

$$S = \frac{\pi}{4} d_0^2 \beta_\infty^2 \tag{8}$$

is the contact surface between splat and droplet (the final spread factor β_∞ is measured from Fig. 6). The variation of the solidification time t_s therefore only depends on $\dot{q}$, i.e., on the product of S (increasing with $T_{2,0}$) and the temperature difference (decreasing with increasing $T_{2,0}$). The coupling of these two opposite trends leads to a minimum in the solidification time. Values of the solidification time calculated by this order of magnitude model described above are plotted in Fig. 9. The value of the effective heat transfer coefficient used in Eq. (7) ($h_e = 4.3 * 10^5$ (W m^{-2} K^{-1})) has been determined by minimizing the differences between the model and the experiments results, in a least square sense. It is worth noting that h_e expresses both the effects of convection in the liquid part of the splat and conductive heat transfer at the splat/substrate interface. These two heat transfer modes have been respectively examined by ([37]) and ([10]) matching experiments with numerical or analytical models. Although the goal of our analytical model is to give a physical explanation of the observed non-monotonic dependence of the solidification time on $T_{2,0}$ and not to provide quantitative results, the estimated value of h_e agrees in an order of magnitude sense with the results of ([10]). The effect of thermal contact resistance on the spreading dynamics cannot be accurately pursued with the present approximate model. A thorough study of this effect has been performed by Xiong et al. [16], who matched the shapes of solidified droplets with the shapes obtained by numerical simulations at different Biot numbers.

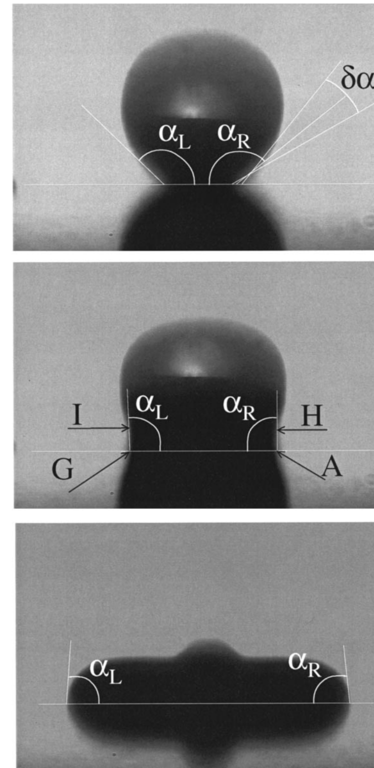

Fig. 10 Determination of the apparent dynamic wetting angles. Angle α_L is determined by points (I,G,A), and angle α_R by (H,A,G). The measurement incertitude $\delta\alpha_R$ comes primarily from the positioning of A and H, its value is estimated +/−12 deg.

3.4 Investigation of the Wetting Dynamics. The visualization method presented here allows the measurement of the evolution of the apparent wetting angle α. This angle is always measured at the contact line between the droplet and the wafer substrate, as shown in Fig. 10, which is a representative frame for our wetting measurements. Each frame allows a double measurement of α, on the left and on the right of the droplet. A graphical estimate in Fig. 10 yields an angular precision of ± 12 deg. It is worth noting that α can only be considered to be a *wetting* angle as long as no solidification has occurred at the contact line. Indicators of the fact that solidification has not occurred are for example the temporal evolution of the spread factor and the temporal variation of the apparent wetting angle. The experimental conditions for the experiments on wetting dynamics are slightly different from the first series of experiments performed in this study, as described above. The time resolution of 300 ns used is well below the jitter due to instabilities in droplet ejection, so we

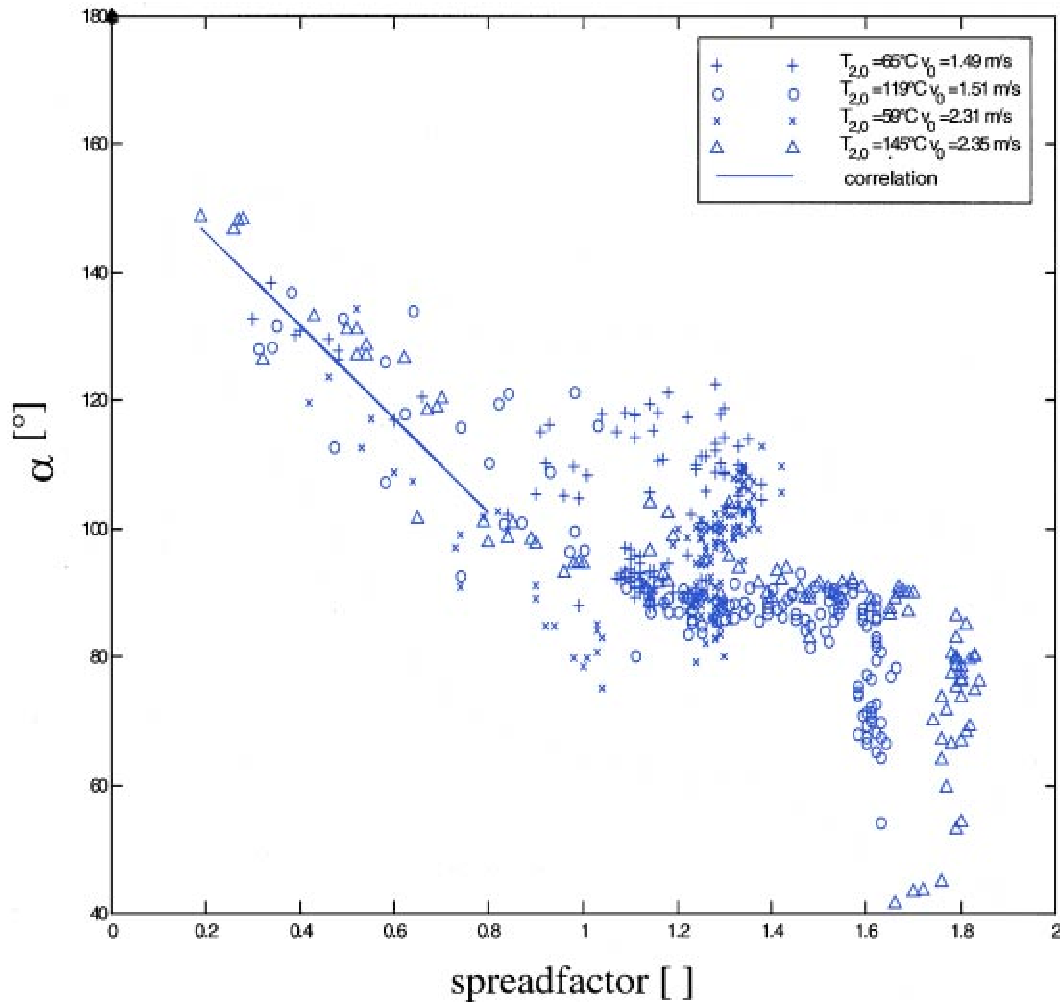

Fig. 11 Evolution of the wetting angle α as a function of the spread factor β for the specified initial substrate temperatures $T_{2,0}$ and impact velocities v_0. The angular error is estimated in Fig. 10.

have selected to base our interpretation of the results on plots of the wetting angle as a function of the spread factor β (Fig. 11) instead of as a function of time (Fig. 12).

Figure 11 shows the evolution of the apparent wetting angle α as a function of the spread factor β for the four cases described in Table 2. These cases differ by the impact velocity v_0 and the initial substrate temperature $T_{2,0}$. At least two regimes can be distinguished in Fig. 11: a first regime where α decreases linearly ($\beta<0.8$), and where the behavior is comparable in the four measurement sequences, and a second regime ($\beta>0.8$), where no consistent behavior for all cases can be observed. In the first regime, measurements and a general optical inspection of the frames do not reveal significant angle and shape differences between the four examined cases, defined by their respective initial impact velocities v_0 and surface temperature $T_{2,0}$: (2.35,145), (2.31, 59), (1.51, 119) and (1.49 m/s, 65°C). A linear curve fit in this first regime yields the following correlation, plotted in Fig. 11:

$$\alpha(\beta)=160\,\mathrm{deg}-71\beta,\beta<0.8. \tag{9}$$

The second regime can be either a horizontal plateau ($\alpha \sim 90\,\mathrm{deg}$) terminated by a region where the value of α oscillates at the maximum value of β as in the case (1.51, 119), or a regime of increase and subsequent decrease of α as in the cases (2.31, 59) and (1.49, 65), where α first increases to a local maximum and then decreases to a final value of about 90 deg (the interpretation of the results in Fig. 11 is aided by plots such as Fig. 12, where time is a coordinate). The last case (2.35, 145) can be viewed as a combination of a plateau and a small zone of increase and subsequent decrease of α for $\beta\in[1.1,1.3]$. It is worth stressing that, although not explicitly extractable from Fig. 11 because time is not a coordinate, oscillations of the value of α at the maximum values of β (for example $\beta=1.6$ and $\beta=1.8$) were observed. Witness to this fact are the frames between 45 and 150 μs in Fig. 5.

The results for α in the first regime can be interpreted as follows. The decrease of the apparent wetting angle value with the spread factor corresponds qualitatively to the predictions of Hoffman's experimental correlation ([12,13]), which expresses that the wetting angle decreases with decreasing capillary numbers (this is the case in the early part of the impact, because the spherical droplet shape induces a contact line velocity that decreases with time):

$$\alpha=f_{\mathrm{Hoff}}(\mathrm{Ca}+f_{\mathrm{Hoff}}^{-1}(\alpha_{eq})) \tag{10}$$

$$f_{\mathrm{Hoff}}(\mathrm{Ca})=4.54\mathrm{Ca}^{0.353}, \quad \mathrm{Ca}<O(0.1). \tag{11}$$

The second term in the parenthesis of Eq. (10) is a correction factor for the influence of the equilibrium wetting angle α_{eq}. Theoretical verification of Hoffman's correlation has been obtained for the case of perfect wetting ($\alpha_{eq}=0$) via hydrodynamic analyses by Voinov and Tanner [38,39]. Equation (11) expresses this correlation for the range of capillary number that pertains to our study [40].

Hoffman suggested analytically that flow inertia could influence α for We>0.015 ([13]). The analyses of Tanner and Voinov

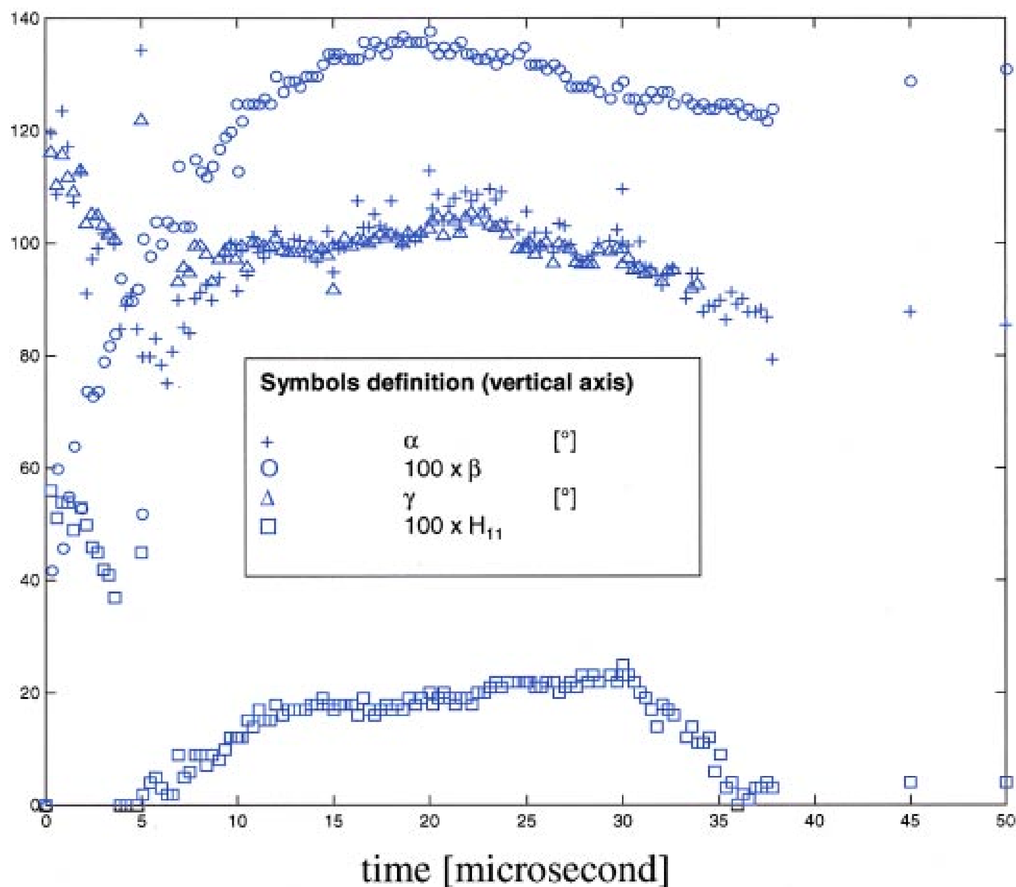

Fig. 12 Time evolution of the spread factor β, the contact angle α, the first ripple angle γ, and the first ripple nondimensional height H_{11} in the case ($v_0=2.31$ m/s, $T_{2,0}=59°C$). The error is estimated in Section 2.3 and in Fig. 10.

focused on the slow viscous flow regime, neglecting flow inertia in the Navier-Stokes equations. Publications can be found stating that inertia effects on the wetting angle can be ignored for Ca $\leq O(0.1)$, without commenting on the influence of the Weber number ([40]). However, most of these wetting studies are performed with high viscosity oils. In the first regime of the droplet spreading observed in this study, the measured contact line velocities of 2–4 m/s correspond to Ca of the order of $1.5*10^{-2}$–$3.2*10^{-2}$, and simultaneously to We of the order of 7 to 28. These moderate Weber number clearly implies that the fluid inertia is not negligible in comparison with capillary forces. This indicates the existence of situations where inertia is not negligible even at low Ca, for example in the case of low viscosity materials such as liquid metals.

A second limitation of Hoffman's correlation and of its hydrodynamic justifications is that they are expressed for steady flows only. Therefore, the application of Hoffman's correlation to an unsteady droplet impact is questionable. However, since Hoffman's correlation is the only widely known available general wetting correlation, it is worth comparing it with our measurements.

Quantitatively, it is difficult to compare the evolution of α with the evolution of the capillary number in this first regime since the equilibrium wetting angle is a prior unknown, and since we only measured an average velocity at the contact line, meaning an average Ca. Assuming an equilibrium wetting angle near zero, these values of Ca of $1.5*10^{-2}$ and $3.2*10^{-2}$ correspond via Eqs. (10)–(11) to wetting angles of, respectively, 59 deg and 77 deg. The assumption of a small equilibrium wetting angle value has been confirmed to some extent in this study experimentally. To this end, we placed on a microheater a wafer slide supporting a solidified solder droplet (80 μm diameter) and heated the slide at 180°C during two minutes. Frames (*a*) and (*b*) in Fig. 13 are top views of the droplet respectively before (at solid state) and at the end of the heating. The drastic increase of diameter of the drop during melting indicates that the melting drop wets the substrate very well creating a film-like structure, corresponding to a small equilibrium wetting angle. We used atomic force microscopy (AFM) in order to quantify the wetting angle value as follows. The slide was removed from the heater right after heating and cooled on a steel surface at ambient temperature in order to freeze the equilibrium wetting angle. It is worth noting that AFM measurements of a liquid surface, in particular of a contact line region at relatively high temperatures are not very reliable and difficult to perform since AFM has been developed for solid surfaces. Implementation in liquid and molten interfaces measurements is at best at its infancy ([41]). The measured values of the frozen contact angle, from the border of the contact line up to nine microns from that line, were smaller than 30 deg (Fig. 13). Even if the equilibrium angle were 40 deg, the dynamic angles values calculated with Hoffman's correlation would only slightly increase (respectively from 59 deg to 65 deg and from 77 deg to 81 deg as discussed earlier), which still does not agree with the measured values that all lie between 90 deg and 140 deg. The fact that a single correlation Eq. (9) could be extracted from impacts with different velocities (Fig. 11) also suggests that Hoffman's correlation is not valid in the first part of the curve describing our measurements. Since Hoffman's correlation does not account for the bulk fluid inertia and the influence of the free surface shape in

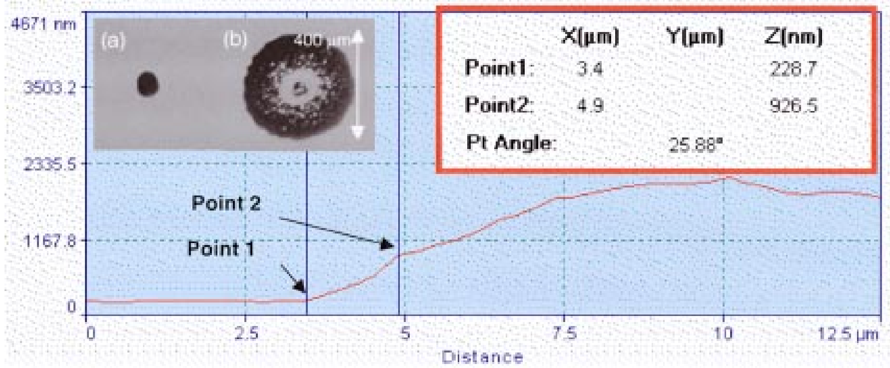

Fig. 13 Contact angle measurement with atomic force microscopy. The two vertical lines determine the position of the angle measurement on the splat profile. Frames (*a*) and (*b*) show the top view of the same (previously solidified) drop before (*a*) and after two minutes heating (*b*) above its melting temperature (180°C).

the vicinity of the contact line, further measurements had to be performed in order to consider the influence of these phenomena on droplet spreading.

The influence of the free surface motion near the wetting angle on this same angle can be examined by tracking the position of the first free surface ripple relative to the contact line. A characteristic free surface point describing the location of the first ripple is the lowest point above the substrate where the horizontal cross section of the droplet reaches a local maximum, represented by point B (*or F*) in Fig. 3 (this point can fall on the contact line, e.g., when the drop has a meniscus shape). An indicator of the influence of the first ripple position on the contact angle α is the angle γ, defined as the angle BAG (or AGF) in Fig. 3. It is worth noting that γ cannot be defined when points B and A (or F and G) coincide. This ''first ripple angle'' γ, when defined, is plotted in Fig. 12 as a function of time for the case (2.31 m/s, 59°C). A clear relation between α and γ during this first part of the spreading is obvious, and is also visible in the three other wetting angle measurement sequences (not plotted in Fig. 12 for clarity), as well as in the frames 2 and 3 of Fig. 5. The nondimensional height of the first ripple above the substrate H_{11} is also plotted in Fig. 12 in order to determine unequivocally the position of the first ripple.

The second regime of the spreading ($\beta > 0.8$) allows a better insight into the relation between γ and α. In Fig. 12 these two angles values exhibit a coordinated increase and subsequent decrease for $t \in [15,30\ \mu s]$. This indicates that the apparent wetting angle and the bending of the free surface over it represented by γ are dependent. This makes sense physically, for example, when one considers the limit case where the contact line freezes suddenly and the first ripple continues to advance because of the bulk fluid flow, as in cases (1.49 m/s, 65°C) and (2.31, 59) in Fig. 11: Here the apparent α will increase only because of the combination between bulk fluid dynamics and heat transfer, and not because of wetting phenomena. Frames 3–5 in Fig. 4 show a similar increase and subsequent decrease of the value of alpha, as in the measurement (1.49, 65). It is worth noting that the apparent receding observed in both low-temperature cases (Fig. 6, Fig. 11, and Fig. 12) is not consistent with the fact that solidification arrests the spreading at low temperature. The exact reasons are not clear to us at the present time.

Another increase and subsequent decrease of the value of α, smaller than in both low-temperature cases, is also observed in Fig. 11 in one high temperature case (2.35, 145). This can also be correlated with a bending of the free surface above the substrate and a corresponding increase of γ. Contrary to both low-temperature cases, this bending is probably caused by the bulk fluid motion instead of solidification, since the latter only affects the motion of the contact line at a later stage. In the other high-temperature case (1.51, 119) the wetting angle remains approximately constant at 90 deg for $\beta > 1$, while the characteristic point describing the location of the first ripple falls on the contact line. This absence of bending of the free surface near the substrate could be explained by an impact velocity lower than in the case (2.35, 145).

We also attempted to test Hoffman's correlation in the second regime for both our high substrate temperature cases. Contact line velocities were estimated to be 1.44 m/s and 0.84 m/s for the cases (2.35 m/s, 145°C) and (1.51, 119), respectively, in the ranges of $\beta \in (1.4,1.8)$ and (1.2, 1.6). These velocities correspond to Ca of $1.1*10^{-2}$ and $6.3*10^{-3}$. The resulting wetting angle values obtained from Hoffman's correlation, assuming again an equilibrium wetting angle of zero, are 53 and 43 deg, respectively. These values differ greatly from the measured values of about 90 deg. It should be noted that this finding is not sensitive to the assumed value of the equilibrium wetting angle: even if the measured equilibrium angle were 40 deg, the wetting angle predicted by Hoffman's correlation would be increased by less than 11 deg, which is far from sufficient to yield agreement with our measurements.

4 Conclusion

To the best of our knowledge, this study presents the first experimental results on the transient fluid dynamics, wetting, and solidification of molten microdroplets impacting on a substrate, which are directly relevant to the novel solder jetting technology in manufacturing of microelectronics. It was shown that the ripples on the solidified drop surface are due to a strong coupling between flow oscillations and solidification, as was suggested by earlier numerical results pertaining to a comparable parameter range ([15,16]). The value of the substrate temperature was varied in order to study its influence on the spreading and solidification process. Transient measurements of the droplet height above the substrate have been carried out, showing a damped oscillation. Our results suggest that the solidification time depends nonmonotonically on the substrate temperature. This finding, although appearing counterintuitive, is supported by a simple order of magnitude analysis. Transient measurements of the spread factor showed that the substrate temperature significantly affects the spreading for substrate temperatures ranging from 48°C to 98°C (Ste = 0.77 to 0.48). This indicates that spreading is arrested by solidification at the wetting line. At higher temperatures, the spread factor was practically independent of the substrate temperature. Measurements of the wetting angle for different conditions of impact velocities and substrate temperature have also been carried out. It was established that the wetting angle dynamics is strongly coupled to the evolution of the droplet free surface and no quantitative agreement with Hoffman's correlation was found. Two successive regimes during the spreading have been

distinguished. The influence of the initial conditions on the evolution of the apparent wetting angle was analyzed in both regimes.

Acknowledgments

This work has been partially supported by the Swiss National Science Foundation (Grant No. 21-49183.96). The authors would like to acknowledge Stefan Haferl whose experience with atomic force microscopy and valuable advice were a great help for realizing the measurement in Fig. 13.

Nomenclature

Ca = capillary number ($\mu v_c \sigma^{-1}$)
c_p = specific heat (J kg^{-1} K^{-1})
d = diameter (m)
E = energy (J)
f = frequency (s^{-1})
h = heat transfer coefficient (Wm^{-2}K^{-1})
H = nondimensional height ((visible height)/d_0)
L = latent heat (J kg^{-1})
Oh = Ohnesorge number ((We)$^{1/2}$/Re)
Pr = Prandtl number ($\mu c_{pl} \lambda_l^{-1}$)
$\dot{q}$ = heat transfer rate (W)
Re = Reynolds number ($\rho v_0 d_0 \mu^{-1}$)
S = surface (m^2)
Ste = Stefan number ($c_{pl}(T_m - T_{2,0}) L^{-1}$)
t = time(s)
T = temperature (K)
V = volume (m^3)
v = velocity (m s^{-1})
We = Weber number ($\rho v_0^2 d_0 \sigma^{-1}$)

Greek Symbols

α = apparent wetting angle
β = spread factor
γ = first ripple angle
Δ = difference
λ = thermal conductivity (Wm^{-1}K^{-1})
μ = dynamic viscosity (Pa s)
ρ = density (kg m^{-3})
σ = surface energy (Jm^{-2})

Subscripts

0 = initial
1 = droplet
2 = substrate top surface
3 = substrate bottom surface
11 = first ripple
c = contact line
e = effective
eq = equilibrium
l = liquid
m = melting point
max = maximum
s = solid, solidification
spr = spreading
∞ = final, arrested

References

[1] Orme, M., 1993, ''A Novel Technique of Rapid Solidification Net-Form Materials Synthesis,'' J. Mater. Eng. Perform., **2**, No. 3, pp. 399–405.
[2] Orme, M., Huang, C., and Courter, J., 1996, ''Deposition Strategies for Control of Microstructures Microporosity and Surface Roughness in Droplet-Based Solid Freeform Fabrication of Structural Materials,'' *Melt Spinning, Strip Casting and Slab Casting*, Matthys, E. F., and Truckner, W. G., eds., The Minerals, Metals and Materials Society, Warrendale, PA, pp. 125–143.
[3] Hayes, D. J., and Wallace, D. B., 1998, ''Solder Jet Printing: Wafer Bumping and CSP Applications,'' Chip Scale Rev., **2**, No. 4, pp. 75–80.
[4] Waldvogel, J. M., Diversiev, G., Poulikakos, D., Megaridis, C. M., Attinger, D., Xiong, B., and Wallace, D. B., 1998, ''Impact and Solidification of Molten-Metal Droplets on Electronic Substrates,'' ASME J. Heat Transfer, **120**, p. 539.
[5] Haferl, S., Zhao, Z., Giannakouros, J., Attinger, D., and Poulikakos, D., 2000, ''Transport Phenomena in the Impact of a Molten Droplet on a Surface: Macroscopic Phenomenology and Microscopic Considerations, Part I: Fluid Dynamics,'' Annu. Rev. Heat Transfer, C. L. Tien, ed.
[6] Attinger, D., Haferl, S., Zhao, Z., and Poulikakos, D., 2000, ''Transport Phenomena in the Impact of a Molten Droplet on a Surface: Macroscopic Phenomenology and Microscopic Considerations, Part II—Heat Transfer and Solidification,'' *Annu. Rev. Heat Transfer.*, C. L. Tien, ed., in press.
[7] Amon, C. H., Schmaltz, K. C., Merz, R., and Prinz, F. B., 1996, ''Numerical and Experimental Investigation of Interface Bonding via Substrate Remelting of an Impinging Molten Metal Droplet,'' ASME J. Heat Transfer, **118**, pp. 164–172.
[8] Bennett, T., and Poulikakos, D., 1994, ''Heat Transfer Aspects of Splat-Quench Solidification: Modeling and Experiment,'' J. Mater. Sci., **29**, pp. 2025–2039.
[9] Pasandideh-Fard, M., Bohla, R., Chandra, S., and Mostaghimi, J., 1998, ''Deposition of Tin Droplets on a Steel Plate: Simulations and Experiments,'' Int. J. Heat Mass Transf., **41**, No. 19, pp. 2929–2945.
[10] Wang, G. X., and Matthys, E. F., 1996, ''Experimental Investigation of Interfacial Thermal Conductance for Molten Metal Solidification on a Substrate,'' ASME J. Heat Transfer, **118**, pp. 157–163.
[11] Blake, T. D., and Haynes, J. M., 1969, ''Kinetics of Liquid/Liquid Displacement,'' J. Colloid Interface Sci., **30**, pp. 421–423.
[12] Dussan, E. B., 1979, ''On the Spreading of Liquids on Solid Surfaces: Static and Dynamic Contact Lines,'' Annu. Rev. Fluid Mech., **11**, pp. 371–400.
[13] Hoffman, R. L., 1975, ''A Study of the Advancing Interface, I—Interface Shape in Liquid-Gas Systems,'' J. Colloid Interface Sci., **50**, pp. 228–241.
[14] Fukai, J., Shiba, Y., Yamamoto, T., Miyatake, O., Poulikakos, D., Megaridis, C. M., and Zhao, Z., 1995, ''Wetting Effects on the Spreading of a Liquid Droplet Colliding With a Flat Surface: Experimental and Modeling,'' Phys. Fluids, **7**, No. 2, pp. 236–247.
[15] Waldvogel, J. M., and Poulikakos, D., 1997, ''Solidification Phenomena in Picoliter Size Solder Droplet Deposition on a Composite Substrate,'' Int. J. Heat Mass Transf., **40**, No. 2, pp. 295–309.
[16] Xiong, B., Magaridis, C. M., Poulikakos, D., and Hoang, H., 1998, ''An Investigation of Key Factors Affecting Solder Microdroplet Deposition,'' ASME J. Heat Transfer, **120**, pp. 259–270.
[17] Inada, S., Miyasaka, Y., Mishida, K., and Chandratilleke, G. R., 1983, ''Transient Temperature Variation of a Hot Wall due to an Impinging Water Drop: Effect of Subcooling of the Water Drop,'' *Proceedings of the Joint ASME/JSME Thermal Engineering Conference*, Vol. 1, ASME, New York, pp. 173–182.
[18] Pederson, C. O., 1970, ''An Experimental Study of the Dynamic Behavior and Heat Transfer Characteristics of Water Droplets Impinging Upon a Heated Surface,'' Int. J. Heat Mass Transf., **13**, pp. 369–381.
[19] Savic, P., and Boult, G. T., 1955, ''The Fluid Flow Associated With the Impact of Liquid Drops With Solid Surfaces,'' Report No. MT-26, Nat. Res. Council Canada.
[20] Toda, S., 1974, ''A Study of Mist Cooling'' (2nd Report: Theory of Mist Cooling and Its Fundamental Experiments), Heat Transfer Japan. Res., **3**, No. 1, pp. 1–44.
[21] Ueda, T., Enomoto, T., and Kanetsuki, M., 1979, ''Heat Transfer Characteristics and Dynamic Behavior of Saturated Droplets Impinging on a Heated Vertical Surface,'' Bull. JSME, **22**, No. 167, pp. 724–732.
[22] Chandra, S., and Avedisian, C. T., 1991, ''On the Collision of a Droplet With a Solid Surface,'' Proc. R. Soc. London, Ser. A, **432**, pp. 13–41.
[23] Stow, C. D., and Hadfield, M. G., 1981, ''An Experimental Investigation of Fluid Flow Resulting From the Impact of a Water Drop With an Unyielding Dry Surface,'' Proc. R. Soc. London, Ser. A, **373**, pp. 419–441.
[24] Wachters, L. H., and Westerling, N. A. J., 1966, ''The Heat Transfer From a Hot Wall to Impinging Water Drop in the Spherical State,'' Chem. Eng. Sci., **21**, pp. 1047–1056.
[25] Mundo, C., Sommerfeld, M., and Tropea, C., 1995, ''Droplet-Wall Collisions: Experimental Studies of the Deformation and Breakup Process,'' Int. J. Multiphase Flow, **21**, pp. 151–173.
[26] Yarin, A. L., and Weiss, D. A., 1995, ''Impact of Drops on Solid Surfaces: Self-Similar Capillary Waves and Splashing as a New Type of Kinematic Discontinuity,'' J. Fluid Mech., **283**, pp. 141–173.
[27] Ohl, C. D., Philipp, A., and Lauterborn, W., 1995, ''Cavitation Bubble Collapse Studies at 20 Million Frames Per Second,'' Ann. Phys. (Leipzig), **4**, No. 1, pp. 26–34.
[28] Levin, Z., and Hobbs, P. V., 1971, ''Splashing of Water Drops on Solid and Wetted Surfaces: Hydrodynamics and Charge Separations,'' Philos. Trans. R. Soc. London, Ser. A, **269**, pp. 555–585.
[29] Hayes, D. J., Wallace, D. B., and Boldman, M. T., 1992, ''Picoliter Solder Droplet Dispension,'' *ISHM Symposium 92 Proceedings*, pp. 316–321.
[30] Arx, M. v., 1998, ''Thermal Properties of CMOS Thin Films,'' Ph.D. thesis, ETH Zurich.
[31] Poulikakos, D., 1994, *Conduction Heat Transfer*, Prentice-Hall, Englewood Cliffs, NJ.
[32] Bennett, T., and Poulikakos, D., 1993, ''Splat-Quench Solidification: Estimating the Maximum Spreading of a Droplet Impacting a Solid Surface,'' J. Mater. Sci., **28**, pp. 963–970.
[33] Schiaffino, S., and Sonin, A. A., 1997, ''Molten Droplet Deposition and Solidification at Low Weber Numbers,'' Phys. Fluids, **9**, pp. 3172–3187.

[34] Fukai, J., Zhao, Z., Poulikakos, D., Megaridis, C. M., and Miyatake, O., 1993, ''Modeling of the Deformation of a Liquid Droplet Impinging Upon a Flat Surface,'' Phys. Fluids A, **5**, pp. 2588–2599.
[35] Schiaffino, S., and Sonin, A. A., 1997, ''Motion and Arrest of a Molten Contact Line on a Cold Surface: An Experimental Study,'' Phys. Fluids, **9**, pp. 2217–2226.
[36] Pasandideh-Fard, M., Qiao, Y. M., Chandra, S., and Mostaghimi, J., 1996, ''Capillary Effects During Droplet Impact on a Solid Surface,'' Phys. Fluids, **8**, pp. S650–S659.
[37] Zarzalejo, L. J., Schmaltz, K. S., and Amon, C. H., 1999, ''Molten Droplet Solidification and Substrate Remelting in Microcasting, Part I—Numerical Modeling and Experimental Varification,'' Heat Mass Transfer, **34**, pp. 477–485.
[38] Tanner, L. H., 1979, ''The Spreading of Silicon Oil Drops on Horizontal Surfaces,'' J. Phys. D: Appl. Phys., **12**, pp. 1473–1484.
[39] Voinov, O. V., 1976, ''Hydrodynamics of Wetting,'' Fluid Dyn., **11**, pp. 714–721.
[40] Kistler, S. F., 1993, ''Hydrodynamics of Wetting,'' Wettability, Berg, J. C., ed., Marcel Dekker, New York.
[41] Haferl, S., Poulikakos, D., and Zhao, Z., 1999, ''Employing Scanning Force Microscopy to Investigate the Dynamic Wetting Behavior of Liquid Microdroplets on Smooth Surfaces: Gathered Experiences,'' Poster Presentation, European Research Conferences (EURESCO) Solid/Fluid Interfaces: Complex Fluid Interfaces, Castelvecchio Pascoli, Italy.
[42] Waldvogel, J. M., Poulikakos, D., Wallace, D. B., and Marusak, R., 1996, ''Transport Phenomena in Picoliter Size Solder Droplet Dispension,'' ASME J. Heat Transfer, **118**, pp. 148–156.